Solar Energy Materials & Solar Cells 270 (2024) 112813

Contents lists available at ScienceDirect

Solar Energy Materials and Solar Cells

journal homepage: www.elsevier.com/locate/solmat

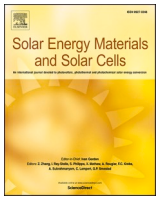

Thin silicon heterojunction solar cells in perovskite shadow: Bottom cell prospective

U. Chime [a,b,*], W. Duan [a], A. Lambertz [a], K. Bittkau [a], V. Lauterbach [a], K. Ding [a], U. Rau [a,b], T. Merdzhanova [a], O. Astakhov [a,**]

[a] IEK-5 Photovoltaik, Forschungszentrum Jülich GmbH, Wilhelm-Johnen Straße, 52425, Jülich, Germany
[b] Jülich Aachen Research Alliance (JARA-Energy) and Faculty of Electrical Engineering and Information Technology, RWTH Aachen University, Schinkelstr. 2, 52062, Aachen, Germany

ARTICLE INFO

Keywords:
Perovskite-silicon tandem
Silicon heterojunction
Thin wafer
Passivation layers
Back reflector

ABSTRACT

Perovskite/Silicon (Pero-Si) tandem with silicon heterojunction (SHJ) bottom cells is a promising highly efficient concept, which in the case of mass production will likely rely on the same wafer feedstock as the single junction Si solar cells. The thickness of these wafers is constantly decreasing for economic and sustainability reasons. We forecast that Si bottom cells for mass produced Pero-Si tandems will be based on wafers thinner than 100 μm. In our work we study challenges and opportunities related to this likely wafer thinning for the performance of the SHJ bottom cells operating in Perovskite shadow. We study SHJ cells prepared on 80 μm thick wafers in comparison to the reference cells based on 135 μm thick wafers addressing two issues: passivation and light management. Effects of passivating layer thickness, back reflector and antireflection coating are studied under AM1.5G standard test conditions, attenuated AM1.5G irradiance, and under Perovskite-filtered spectrum. We show that major wafer thickness reduction of 40% turns to only approx. 0.35%$_{abs}$ loss in the bottom cell efficiency. This minor loss can be reduced even further using highly technological ITO/MgF_2/Ag back reflector and MgF_2 anti-reflection coating. Our work shows that significant potential for Pero-Si tandems is waiting to be explored in the perovskite shadow from the SHJ bottom cell perspective.

1. Introduction

Single junction solar cells based on crystalline silicon (c-Si) dominate the photovoltaic market with the present maximum efficiency of 26.7% [1] being few absolute percent away from the theoretical efficiency limit [2]. Further progress in efficiency is expected from the multi-junction tandem solar cells comprising of two or more semiconductor materials of different bandgaps [3–5]. Perovskite/Silicon (Pero-Si) is the most promising tandem combination in terms of efficiency, cost, and scalability for terawatt production scale [6–10]. The Pero-Si concept relies on the highly developed Si bottom cell and therefore, the mass-produced tandems will rely on the same wafer feedstock as the single junction Si solar cells [11,12]. The thickness of these wafers has reduced consistently from 400 μm in 1990 [13] to approximately 150 μm at present and it is forecasted that the wafer thickness will continue to reduce at least during the next decade [12]. The reduction is motivated by the reduction of material usage, costs, CO_2 footprint [13] and supply chain resilience. For example, the European Commission considers Si as both a strategic and a critical raw material for green energy transition [14]. Therefore, we believe that future Si-bottom cells for Pero-Si tandems will be manufactured on wafers thinner than 100 μm. The main motivation for this work is to study implications of wafer thinning on the performance of the bottom Si cell operating in Perovskite shadow. More specifically the study is focused on Si heterojunction solar cells (SHJ) as the most prominent bottom cell partner for Perovskite solar cells [12].

In our previous work, we have already studied the effects of wafer thickness on standalone SHJ solar cells [15]. Our conclusions in line with similar studies [16–19], indicate that besides expected reduction in infrared current, thinning of the wafers increases the open-circuit voltage (V_{OC}), pushing it to the Auger limit, while the fill factor (*FF*) is affected by the recombination losses related to imperfect surface passivation.

In this work, we study performance of SHJ cells prepared on 80 μm thick wafers under the bottom cell conditions in Pero-Si tandem. These

* Corresponding author. IEK-5 Photovoltaik, Forschungszentrum Jülich GmbH, Wilhelm-Johnen Straße, 52425, Jülich, Germany.
** Corresponding author.
E-mail addresses: u.chime@fz-juelich.de (U. Chime), o.astakhov@fz-juelich.de (O. Astakhov).

https://doi.org/10.1016/j.solmat.2024.112813
Received 22 November 2023; Received in revised form 12 March 2024; Accepted 12 March 2024
Available online 16 March 2024

"thin cells" are compared to the ones prepared on more common 135 μm thick wafers. We particularly aim to reveal challenges and opportunities for thin SHJ cells hidden in perovskite cell shade. The utilization of thin wafers for the bottom cells is generally associated with reduced infrared response due to the light path length reduction [2,15]. At the same time, the reduced intensity and narrower, lower energy photon spectrum received by the bottom cell (Fig. 1(a)), relaxes some of the optical and electrical constraints on the functional layer stack of the SHJ solar cell. This in turn opens opportunities for SHJ cells optimization that were inaccessible in the single junction configuration. These issues are addressed in our work, bearing in mind that any optimization measures should be easily implementable into the existing production process chain.

First we revisit one of the major losses in crystalline Si solar cells associated with recombination at the interfaces between the wafer and the stack of carrier selective layers [21]. The core of SHJ technology is the efficient passivation of the Si surfaces using intrinsic hydrogenated amorphous silicon (<i>a-Si:H) layers [22]. In most cases, the passivation quality improves with the thickness of the passivating layers, boosting the implied open circuit voltage (iV_{OC}) and implied fill factor (*iFF*). However, increase in the a-Si:H layer thickness simultaneously leads to increase in optical losses via parasitic absorption, particularly in the short wavelength region, and fill factor losses due to the increase in series resistance [23–26]. When switching from single junction to bottom cell operation, the high energy light is blocked by the top cell and the parasitic absorption in the short wavelength region is no longer an issue. Concurrently, lower light intensities received by the bottom cells proportionally reduce the significance of the series resistance in the stack [27,28]. Therefore, we investigate the effect of thicker passivating layers in SHJ solar cells based on thinner wafers, for Pero-Si tandem applications.

The issue of the photocurrent loss in the near-infrared absorption region in thin wafer Si solar cells [2,15] is addressed with two strategies. Firstly, we consider light trapping options to reduce the transmission of the infrared light through the rear side. While variety of advanced architectures exist for efficient light trapping [29–33], simple solutions such as optimized one-dimensional back reflector are preferrable for large scale production. Full back Ag layer deposited directly on indium tin oxide (ITO) at the rear side is a common one-dimensional back reflector option. The issue of the parasitic plasmonic absorption at the transparent conductive oxide (TCO)/metal interface [34,35] can be mitigated with an additional interlayer of a low refractive index dielectric material such as MgF_2 [34]. The second strategy to minimize the infrared absorption loss in thin wafers is the deposition of an anti-reflection coating on the front side with thickness optimized to promote the transmittance of infra-red light to the bottom cell. For example MgF_2 is considered a suitable material for anti-reflection not only for SHJ solar cells [36] but also in perovskite/silicon tandems [37]. While the MgF_2 coating may perform differently when deposited directly on the SHJ front side, the perovskite front side or even in the case of encapsulation with another material, in this paper, we only demonstrate the possibility to improve infrared light absorption in thin SHJ bottom cells via antireflective coating optimization.

This study consists of two sections dedicated to *passivation* and *light management*. In the "passivation" section we study the passivation layer thickness effect on the performance of SHJ cells prepared on 80 μm thick wafers in comparison to 135 μm thick reference. These cells will be referred to as "80 μm cells" and "135 μm cells", respectively, for the sake of brevity. First the 80 μm and 135 μm cells are compared under AM1.5G standard test conditions. Then, these cells are studied under perovskite-filtered spectrum - the spectrum a bottom cell would experience in Pero-Si tandem under AM1.5G standard test conditions. This spectrum is obtained as a product of the standard AM1.5G spectrum and transmittance of perovskite solar [20] cell shown in Fig. 1(b). Additionally, to resolve any spectrum-specific influence on the operation of the SHJ cells we compare measurements done under the "Perovskite-filtered" spectrum to the measurements under AM1.5G spectrum attenuated so that the cells received same total photon flux in both cases.

In the second "light management" section, we address the application of the one-dimensional back reflectors and the MgF_2 anti-reflection coating to improve light trapping in SHJ bottom cells based on thin and reference wafers with different thickness of the passivation layer from the first part of the study.

2. Experimental details

The silicon heterojunction solar cells were fabricated using Czochralski-grown M2 n-type <100 > c-Si wafers with resistivity of 1 Ωcm. To remove saw damage, the c-Si wafers were chemically etched, and then textured on both sides to produce random pyramids using diluted KOH. After texturing, the wafers were cleaned using a solution of HCl, O_3 and H_2O. Thinner wafers were obtained by increasing saw damage removal time and the thickness was estimated using the weight of the wafer. The plasma-enhanced chemical vapor deposition (PECVD) process was used to deposit a stack of intrinsic/n-type hydrogenated amorphous silicon (a-Si:H) on the front side and intrinsic/p-type a-Si:H on the rear side. On both sides of the wafers, ITO was sputtered from a 3% Sn-doped In_2O_3 target. The silver grid contacts were printed on both sides and cured at 170 °C for 40 min to produce bifacial cells. For the back reflectors, the MgF_2 was evaporated on the rear side and subsequently, 200 nm of Ag was sputtered to cover the full rear side. After screen printing and the Ag full-back sputtering, the cells were treated to

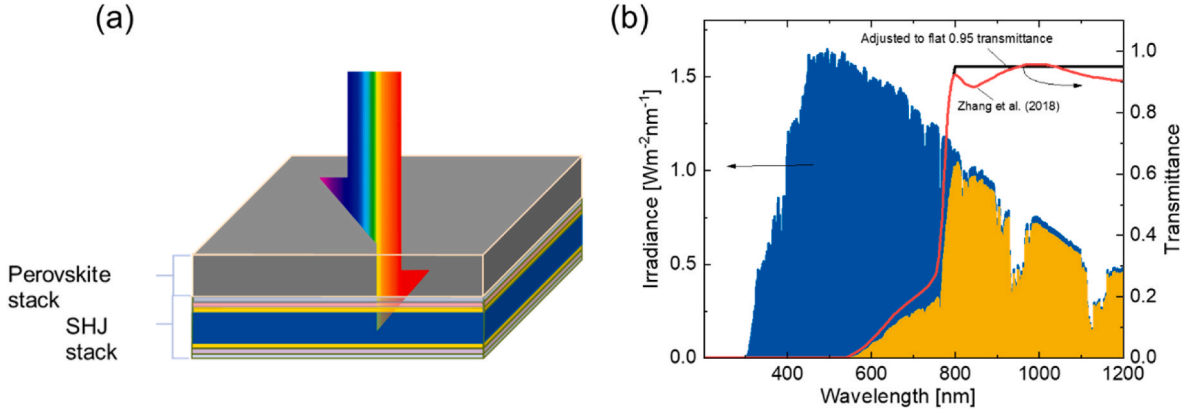

Fig. 1. (a) Simplified perovskite/silicon schematic showing the transmission of infrared light to the bottom silicon heterojunction solar cell; (b) Perovskite-filtered spectrum obtained as a product of the solar spectrum and the transmittance of perovskite solar cell reported by Zhang et al. [20] and adjusted to 95% transmittance from 800 nm to 1200 nm.

a simultaneous light-soaking and annealing process at an intensity of 55 kW/m^2 and at a temperature of 190 °C for 90 s. Finally, MgF_2 with a thickness of 110 nm was evaporated directly on the front ITO as a second anti-reflection coating for all cells.

After the deposition of the passivation, doped and ITO layers but prior to contact printing, all samples were characterized for excess carrier lifetime with the Quasi Steady State Photoconductance (QSSPC) measurements performed using Sinton system. Implied open circuit voltage iV_{OC} and implied fill factor i*FF* values were determined out of the QSSPC measurements. LOANA solar cell analysis system from pv-tools equipped with a Wavelabs Sinus 220 light source were used to measure the current-voltage characteristics under standard test conditions with an AM1.5G and under perovskite-filtered spectra. To produce the perovskite-filtered spectrum the LED source of the LOANA system has been reprogrammed to match transmission spectrum of a semi-transparent perovskite solar cell reported by Zhang et al. [20] and adjusted to 95% from 800 nm to 1200 nm as shown in Fig. 1(b). In addition to standard IV-measurements, J_{SC}-V_{OC} measurements have been taken with LOANA to determine pseudo-*FF* of the cells. The external quantum efficiency (EQE) and reflectance (Ref) were measured on a 20 by 20 mm^2 area on the cells with the printed contact grids.

3. Results and discussion

3.1. Passivation

In this section, we study effect of passivation layer thickness on 80 μm and 135 μm SHJ solar cells under AM1.5G, attenuated AM1.5G, and perovskite-filtered spectra. The structure of the SHJ solar cell is schematically presented in Fig. 2(a). Each passivation layer on both sides of the wafer consists of two films of intrinsic hydrogenated amorphous silicon. The first layer (i1) is a rapidly deposited porous buffer layer which prevents epitaxial crystallization on the interface and a denser second layer (i2) is deposited to make up the actual passivation layer [34]. Only the i2 layer thickness is varied in this study by tripling the deposition time on the front side and/or doubling the deposition time on the rear side as shown in the table in Fig. 2(b).

Note that for brevity as listed in Fig. 2(b) we will address the cells with reference thickness of the i-layer as "standard", the cells with thicker i-layer at the p-side as "p-side cells", the cells with thicker i-layer at the n-side as "n-side cells" and finally when both are thicker the cells are called "both sides cells".

The performance of the 80 μm and 135 μm cells with the different passivation layer thickness combinations before light curing and annealing is summarized in Fig. 3. In Fig. 3(a) we can see that under AM1.5G the solar cells made on thinner wafers produce higher open-circuit voltage (V_{OC}) compared to the thicker cells [15,16] because of increased excess charge carrier concentration in thinner wafers [2,15,16]. The lower implied fill factor (i*FF*) in thin cells in Fig. 3(b) is attributed to increased impact of the surface recombination and reduced short-circuit current density (J_{SC}) in Fig. 3(c) is a result of reduced IR light absorption in thiner wafers. Detailed discussion on the wafer thickness effect on silicon heterojunction solar cells is presented in the literature [15,16]. Under AM1.5G, the 80 μm cells with standard passivation gain approximately 4.4 mV in V_{OC} over the 135 μm cells of the same passivation and lose about 0.37 mA/cm^2 in J_{SC}.

From the passivation layer thickness point of view, as expected, the highest iV_{OC} of 758 mV and i*FF* of 86.4% were obtained for the "both sides" cells. This is attributed to the reduced surface recombination on both interfaces passivated with thicker amorphous silicon layers. However, the "n-side" 80 μm did not show any improvement in iV_{OC} and V_{OC} compared to the "standard" reference passivation thickness, contrary to expectations. The iV_{OC} and V_{OC} values in "p-side" cells are even below those of the "standard" passivation stack. The reason for this is not fully understood. We tentatively attribute this inconsistency to the batch-to-batch variability in the wafer thinning process. This is indirectly confirmed by the more consistent behavior of iV_{OC} and V_{OC} in the reference cells on 135 μm thick wafers.

Similar drops between iV_{OC} and V_{OC} (approx. 0.18 mV for 80 μm and 0.11 mV for 135 μm cell thickness) in all samples, suggest similar contact recombination loss irrespective of the passivation layer thickness. In general, increasing the passivation thickness on either side of the solar cell is expected to increase series resistance loss. This can be seen in Fig. 3(b) where on average, the difference between pseudo-*FF* (p*FF*) and *FF* is smallest for the standard cells (2.7%$_{abs}$) which have the thinnest passivation layers amongst all cell variants. Interestingly, a higher p*FF* to *FF* loss is observed for the both sides (4.0%$_{abs}$) and the p-side (4.1%$_{abs}$) cells than the n-side cells (3.2%$_{abs}$) which indicates that thicker passivation layer at the n/i/p junction contributes stronger to series resistance than at the n/i/n interface.

With thicker passivation on both sides, an additional 4.7 mV in V_{OC} is gained for the 80 μm cells over the 80 μm cells with standard passivation. However, this gain in V_{OC} is counterbalanced by an additional J_{SC} loss of about 0.40 mA/cm^2 which results in a slightly lower final efficiency for both sides variant (22.7%) compared to the standard variant (22.8%) for the 80 μm cells. At this cell development stage, the best 135 μm cell efficiency is approximately 0.5%$_{abs}$ greater than the best 80 μm cell.

Overall, as might be expected, there is no advantage of the thicker passivating layer under AM1.5G irradiance, and thinner wafers show a mild drop in efficiency. At the next stage, the full set of samples presented in Fig. 3 has been exposed to the light soaking (LS) and

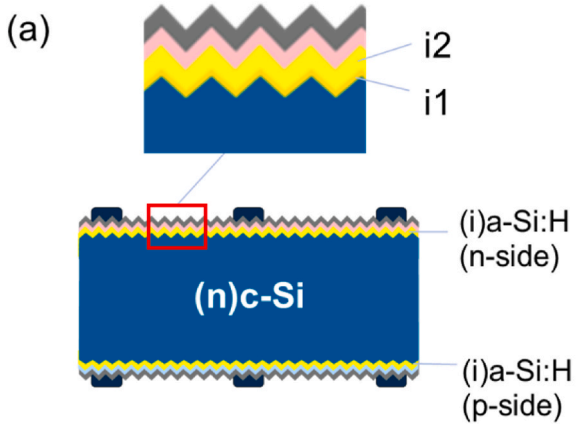

(b)

Front \ Rear	Baseline	2 x i2
Baseline	**standard**	**p-side**
3 x i2	**n-side**	**both sides**

Fig. 2. (a) Silicon heterojunction solar cells schematic showing the two intrinsic amorphous silicon passivation layers; (b) passivation layer thickness variations on the front and/or rear side studied.

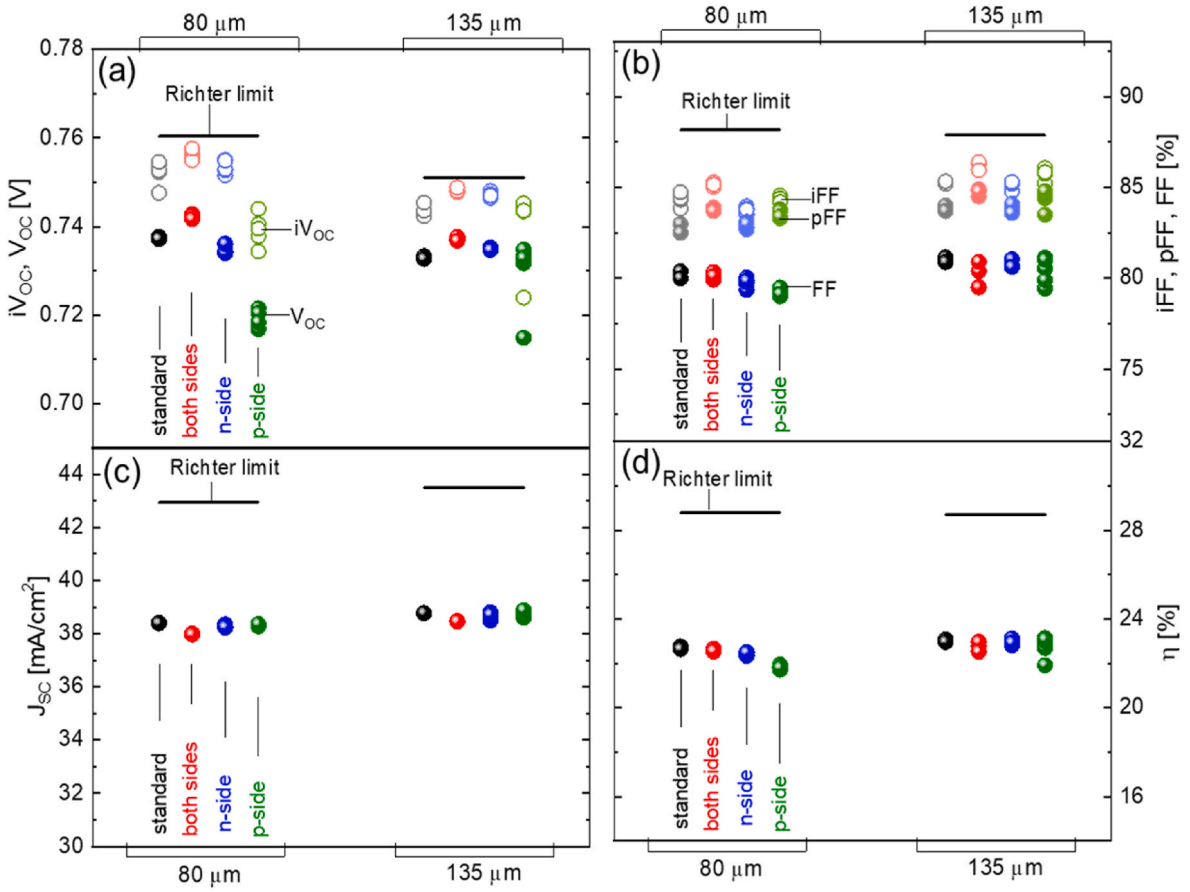

Fig. 3. (a) Implied open circuit iV_{OC} and open-circuit voltage V_{OC}; (b) i*FF*, p*FF*, and *FF*; (c) short-circuit current density J_{SC}; and (d) efficiency η plotted for the different passivation layer variations for wafer thicknesses of 135 and 80 µm under AM1.5G spectrum and before light soaking and annealing process. Solid black lines represent the theoretical limit [2].

subsequent annealing.

Hydrogenated amorphous silicon is prone to the creation of additional defect states under light exposure. This effect, known as the Staebler-Wronski effect [38] is detrimental for efficiency in thin film Si solar cells [38] and has been reported for light-soaked i/c-Si/i interface structures [39]. However SHJ cells with doped amorphous Si layers deposited on either side on contrary have been reported to gain in passivation quality after light exposure [39]. In Fig. 4(a), we compare the results of the full set of samples before and after the light soaking and annealing. All samples show increase in V_{OC} after the LS and annealing with the most gain of up to 22.2 mV in the p-side 80 µm cells which had lowest V_{OC} values before LS treatment. Both sides cells show the highest V_{OC} of 747 mV in 80 µm cells and 741 mV in 135 µm cells. The gain in V_{OC} after LS and annealing is approximately 5.3 mV for 80 µm and 4.8 mV for 135 µm cells (lowest in these cells among the whole sample set). We speculate that these cells are approaching Auger-recombination-dominated regime where further increase in V_{OC} becomes more challenging as it has been demonstrated earlier [15]. Similarly, for the p*FF* in Fig. 4(b), the least gains ranging from 0.4 to 0.7%$_{abs}$ are observed for both sides cells of 80 µm thickness.

As we can see in Fig. 4(b) in all cell types and thicknesses, the LS and annealing improves *FF* (up to 1.9%$_{abs}$) stronger than the p*FF* (max. 1.3 %$_{abs}$), which indicates improvements not only in the passivation but also in the conductivity of the cells. While the light soaking process has little to no effect on the J_{SC} of the 135 µm cells in Fig. 4(c)–a slight loss in J_{SC} is observed for the thinner cells and the reason for this loss is not understood. Overall gains in V_{OC} and *FF* result in efficiency gain for all cell types with the most gain of 0.98 %$_{abs}$ and 0.88 %$_{abs}$ observed for the p-side variants of 80 µm and 135 µm, respectively. At this point, under the AM1.5G irradiance, the best 80 µm cell with an efficiency of 23.3 % is the cell with standard passivation while the best 135 µm cell with an efficiency of 23.8 % is the cell with thicker passivation on p-side.

After the standard test conditions, we approach the operating conditions in the Pero-Si tandems by addressing firstly, the effect of irradiance. Representative cells of each type have been characterized under AM1.5G spectrum attenuated in several steps. Fig. 5 shows the dependencies of the photovoltaic parameters on irradiance for the standard and both sides cell types prepared on 135 and 80 µm thick wafers. In Fig. 5(a) the dependence of V_{OC} on irradiance is presented. The "both sides" thicker passivation cells show consistently higher V_{OC} on reference and thin wafers. The dependencies in Fig. 5(a) show a gradual change in slope from steeper at low intensity to flatter at high intensity i.e., intensity dependent diode ideality factor. The thin wafer cells have somewhat steeper dependencies as compared to the standard wafer counterparts. The results are in qualitative agreement with our previous findings [15]. The gain in V_{OC} attained in thin wafer cells in Fig. 5(a) is highest at one sun and reduces with reduction of intensity. Nonetheless, at 0.44 suns, which is the expected light intensity under the perovskite-filtered spectrum, the 80 µm cells still show 3–5 mV higher V_{OC} compared to the 135 µm reference.

Fig. 5 (b) shows dependencies of *FF* on irradiance. From a wafer thickness perspective, the thinner wafer loose approximately 1%$_{abs}$ of *FF* for the whole range of irradiance as compared to the reference cells. This is due to the stronger impact of the SRH surface recombination in thinner cells [15]. From the perspective of the passivation layer thickness, despite the two variations (standard and both sides) having similar values under 1 sun irradiance, a clear gain in fill factor is observed for the both-sides variant at lower intensities, clearly showing the effects of

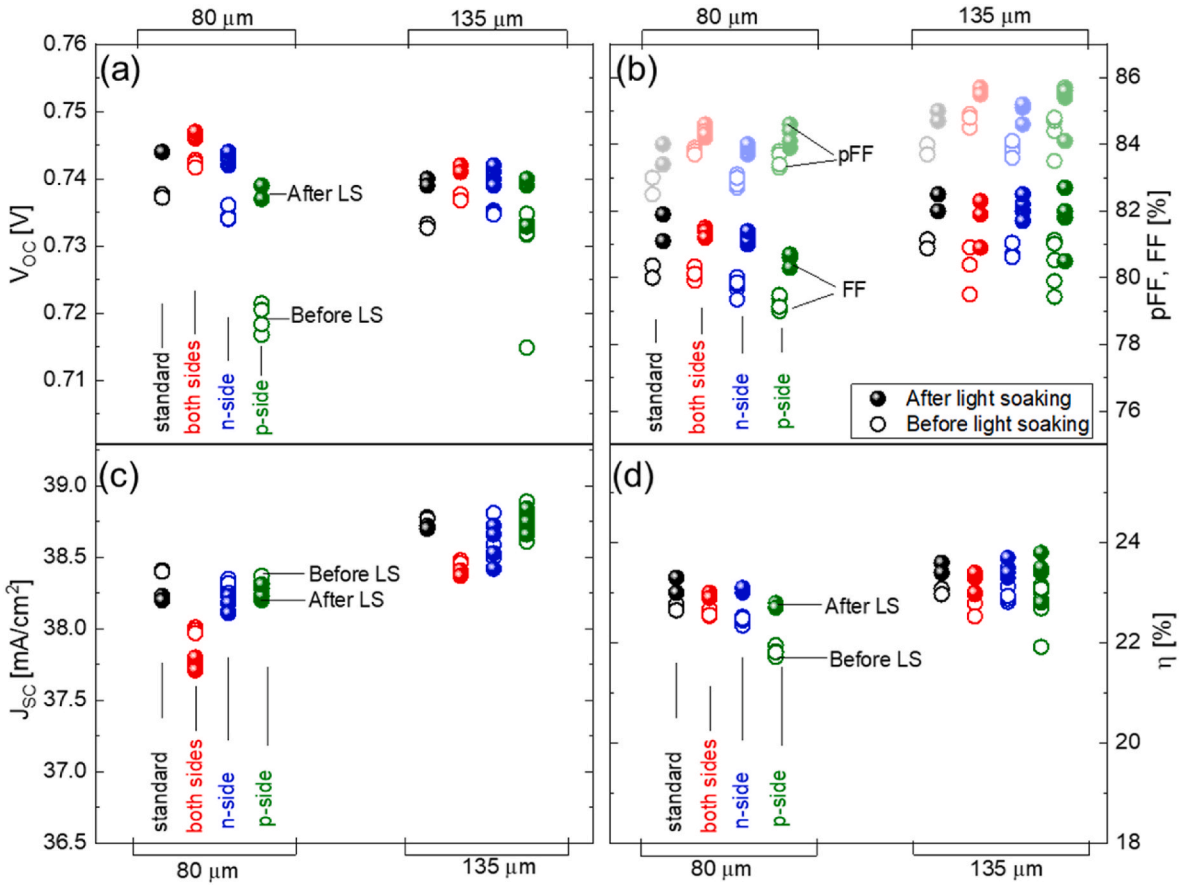

Fig. 4. (a) Open-circuit voltage V_{OC}; (b) pseudo fill factor p*FF* and fill factor *FF*; (c) short-circuit current density J_{SC}; and (d) efficiency η plotted for the different passivation layer variations for wafer thicknesses of 135 and 80 µm under AM1.5G spectrum. All values measured before and after light soaking and annealing.

improved passivation which has been masked by the series resistance under one sun. Here, we can see the example of the *FF* gain achieved thanks to relaxed series resistance constrains in SHJ cell in perovskite shadow.

Fig. 5(c) shows a very consistent linear dependence of J_{SC} on the irradiance for all cells. At this light intensity, the J_{SC} for cells with thicker passivation on both sides remain slightly less than that of the cells with standard passivation thickness, however, under perovskite-filtered spectrum, we expect no additional losses due to thicker passivation on the front side. Despite being slightly lower under AM1.5G, the final efficiency with respect to incident light intensity in Fig. 5(d) shows higher values for the cells with thicker passivation on both sides than the standard cells with differences of 0.1%$_{abs}$ for 80 µm and 0.15%$_{abs}$ for 135 µm cells at the studied light intensity.

Finally, we compare all cells under the target Perovskite-filtered spectrum and the results are presented in Fig. 6. To study possible spectral related effects, we compare the performance of the cells under the perovskite-filtered spectrum to the measurements under AM1.5G spectrum attenuated to the same photon flux (0.44 suns). Both spectra are presented in Fig. 7. We can see in Fig. 6(a) and (b) that both attenuated and Perovskite-filtered spectra result in same V_{OC}, p*FF*, and *FF*. We can conclude that significant modification of the spectrum does not have any effect on the V_{OC} and *FF*. This fact is of interest to streamline further development of the SHJ bottom cells for tandem applications. Primary optimization loop for the V_{OC} and *FF* in these cells can utilize simple attenuation of the typical solar simulator irradiance without modification of the spectrum and building actual tandem cells.

For the 135 µm cells, a slight increase in J_{SC} of approx. 0.33 mA/cm^2 is observed in Fig. 6(c) under the perovskite-filtered spectrum in comparison to the attenuated AM1.5G. Here, we observe the reduced parasitic absorption of the short wavelength light which is absent in the Perovskite-filtered spectrum. For the 80 µm cells however, little to no gain in J_{SC} is noted. We conclude that two counterbalancing effects take place in this case. On the one hand, the losses in the short wavelength region are absent so there is a net gain in current. On the other hand, the J_{SC} loss due to the transmission losses is magnified in the near infra-red range. This is because for same photon flux, the Perovskite-filtered spectrum has a higher spectral density in the near infrared region than the attenuated AM1.5G as can be seen in Fig. 7. Reduction in EQE in 80 µm cells is presented in Fig. 7 as well. Final efficiencies presented in Fig. 6(d) do not show any definite trend among all passivation layer variants. There is an average loss of approx. 0.35%$_{abs}$ when wafer thickness is reduced from 135 µm to 80 µm.

This result looks optimistic for the thin wafer bottom solar cells. We can see that major wafer thickness reduction of 40% turns to only approx. 0.35%$_{abs}$ lost in the bottom cell efficiency. This makes application of 80 µm wafers viable for the Pero-Si tandems in future. Based on the passivation study, relaxed optimization conditions to the optical absorption in the thin film Si stack allows increase of the passivation layer thickness with related gain in passivation quality. As our study covered only a little fraction of all stack optimization options, we expect more potential to be discovered in future studies. As the major difference between 135 µm and thin 80 µm cells is in the near IR absorption loss, we elaborate on this topic in the second part of our study.

3.2. Light management

Thin wafer silicon solar cells experience increased losses in infrared light due to the reduced optical path length as shown in J_{SC} results discussed in the previous section. To improve absorption of the low

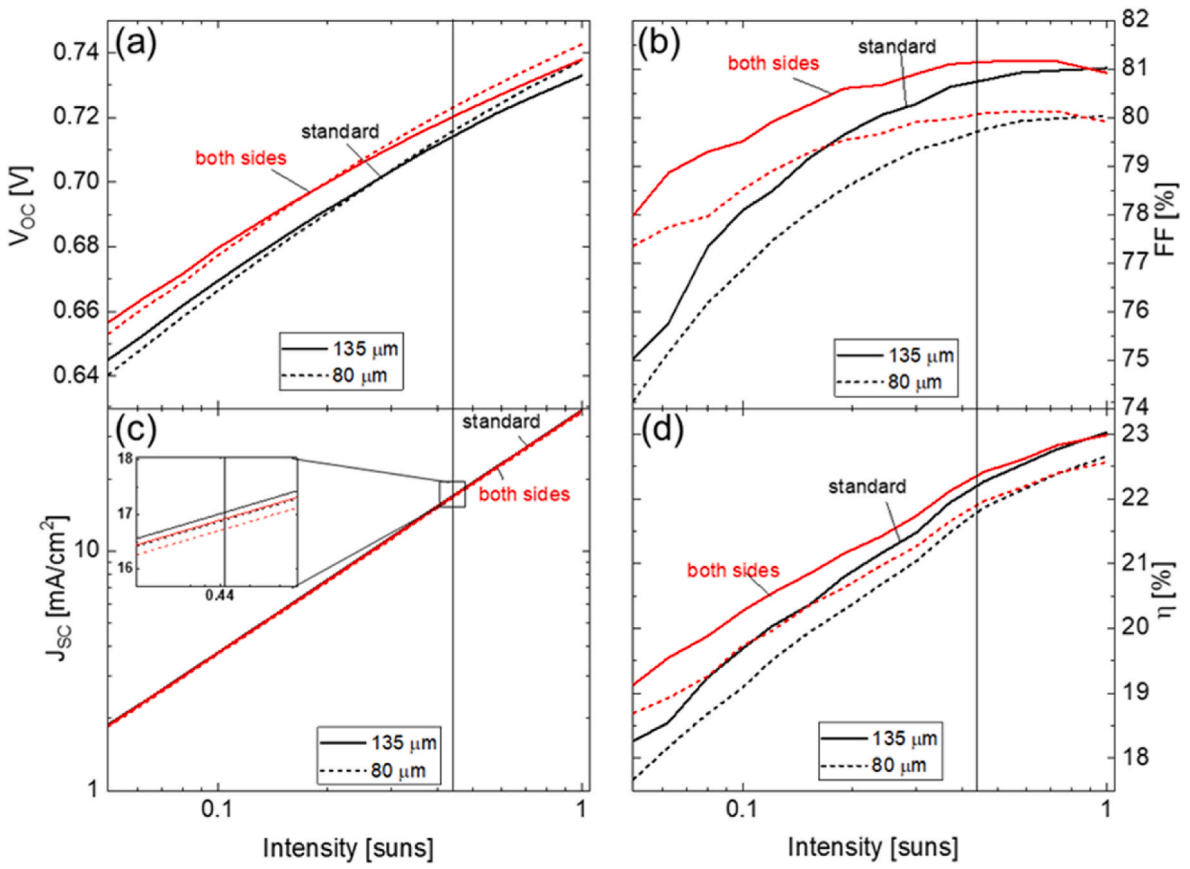

Fig. 5. Intensity dependence of (a) V_{OC}; (b) *FF*; (c) J_{SC}; and (d) η plotted for standard and both sides variations and for wafer thicknesses of 135 and 80 μm.

energy light in this study, we employ two strategies: (i) one-dimensional back reflectors and (ii) anti-reflection coating facilitating transmittance of infra-red light to the bottom cell. In the optimization run several BR stacks of ITO/Ag and ITO/MgF_2/Ag have been tested on reference 135 μm cells. Schematic presentation of the BR stack and its effect on J_{SC} are presented in Fig. 8. To obtain the relative difference in $J_{SC,}$ the cells were first measured using a black chuck before the deposition of BR stacks. Our result shows that the stack of 70 nm ITO with MgF_2 produces the most gain in J_{SC} (0.61 mA/cm^2) outperforming the stack of directly sputtered Ag on ITO (0.42 mA/cm^2) in agreement with earlier findings [34]. It can be seen in Fig. 8 (b) that increase in ITO layer thickness only results in increased parasitic absorption loss.

The best performing BR stack (ITO 70 nm + MgF_2 160 nm + Ag 200 nm in Fig. 8(b)) was then deposited on all samples studied in the previous section. Subsequently, all samples were finalized with MgF_2 ARC. Results of J_{SC} measurements before BR, after BR, and after ARC are presented in Fig. 9. The left graph Fig. 9(a) presents values measured under AM1.5G, and the right graph Fig. 9(b) presents values measured under the perovskite-filtered spectrum. We can see a significant effect of BR leading to improvement in J_{SC} for all cell types under both AM1.5G and Perovskite filtered spectra. The same is true for the ARC, which boosts J_{SC} of all cells.

To get a more detailed view on the effect of both back reflector and antireflective coating, the differential J_{SC} gain is presented in Fig. 10. The left diagram Fig. 10(a) presents data on J_{SC} gain after the deposition of BR. The right graph Fig. 10(b) presents the J_{SC} gain attained at the next step after ARC deposition. As it can be expected most gain in J_{SC} after BR application is attained in the cells with most near IR losses, namely the 80 μm solar cells gain up to 0.88 mA/cm^2 under AM1.5G and up to 0.58 mA/cm^2 under the Perovskite-filtered spectrum after the application of BR. In the same respective cases, the 135 μm cells gain 0.73 mA/cm^2 and 0.52 mA/cm^2. It seems to be practically feasible to reduce the difference between 80 μm and 135 μm cells even further with more advanced back reflectors. Results on the J_{SC} gain after MgF_2 ARC deposition presented in Fig. 10(b) show no distinct trend. All cells gain on average approx. 0.3 mA/cm^2 for both spectra because applied ARC is designed to perform best in the long wavelength range which is approx. same for both spectra. We emphasize here that the ARC applied in our experiment was effective at the air/cell interface and further ARC optimization may be required in the case of monolithic PeroSi tandems. In total, in the cells with thicker passivation layer on both sides, J_{SC} gains of up to 1.2 mA/cm^2 and 0.9 mA/cm^2 were obtained under AM1.5G spectrum for 80 μm and 135 μm wafers, respectively.

The external quantum efficiency (EQE) and absorptance (1-Ref) spectra for representative 80 μm cells are summarized in Fig. 11. Different variants of passivation layer thicknesses presented in Fig. 11(a) show mostly variations in the short wavelength region. Thicker passivation layer increases parasitic absorption loss in the wavelength region between 350 and 600 nm. We can see that the infra-red EQEs and whole 1-Ref spectra of all cells are not affected by the variations in the passivating layers in our work. Therefore, under the PeroSi tandem conditions, the differences in J_{SC} between the different passivation variations are minimal. From a light management perspective in Fig. 11 (b), the introduction of a back reflector enhances the absorption of long wavelength light. This improvement can be observed in the enhanced EQE curve which initiates at approximately 900 nm wavelength. Note that for the cell without back reflector, the "1-Ref" curve in the 1100–1200 nm range is higher than that of the cell "with BR". This observation can presumably be explained by the rear transmission loss in the cell without BR, which is suppressed by the introduction of the back reflector. After the deposition of MgF_2 ARC, further improvement in EQE is observed in the UV region between 340 nm and 480 nm and in the near IR region between 700 nm and 1040 nm. This is indicative of the potential for MgF_2 antireflective coating to improve infrared light

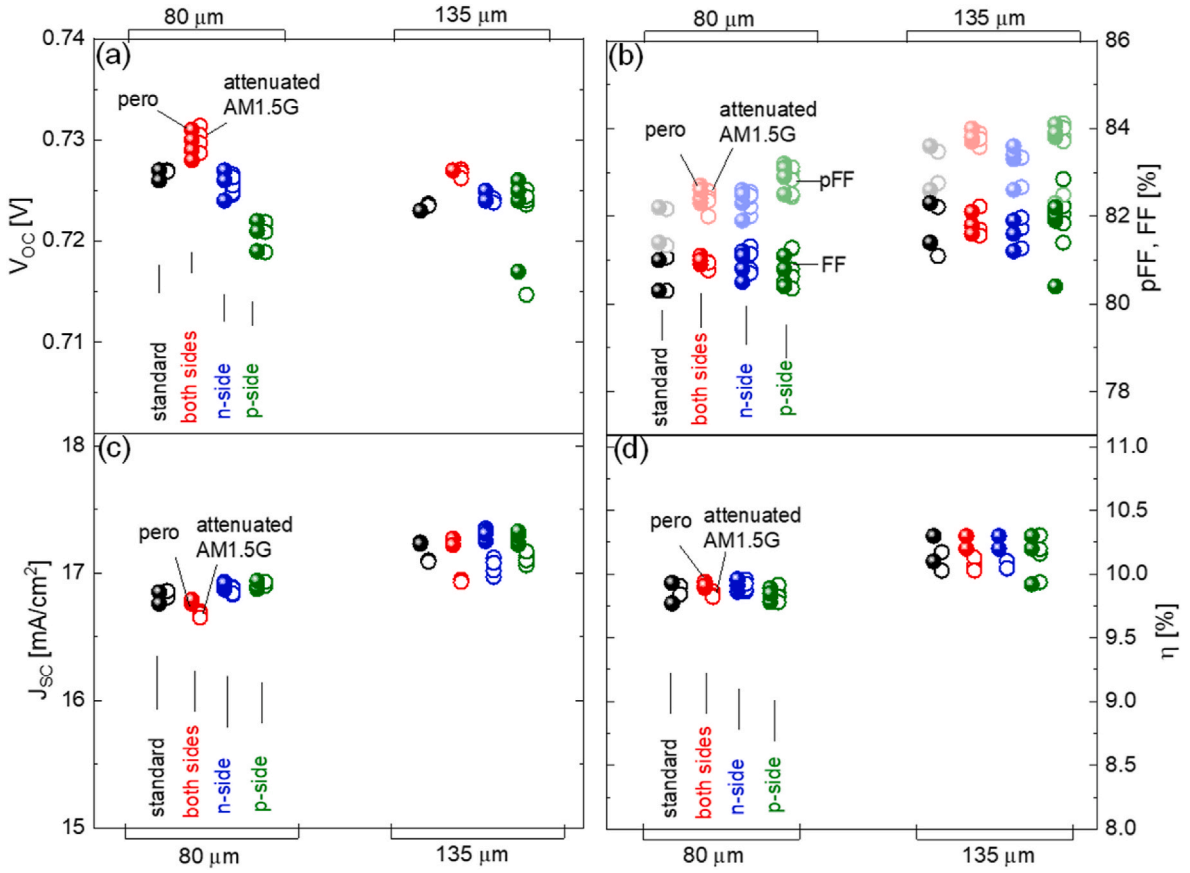

Fig. 6. (a) Implied open circuit iV_{OC} and open-circuit voltage V_{OC}; (b) i*FF*, p*FF*, and *FF*; (c) short-circuit current density J_{SC}; and (d) efficiency η plotted for the different passivation layer variations for wafer thicknesses of 80 and 135 µm under perovskite-filtered spectrum and under AM1.5G spectrum at the same intensity.

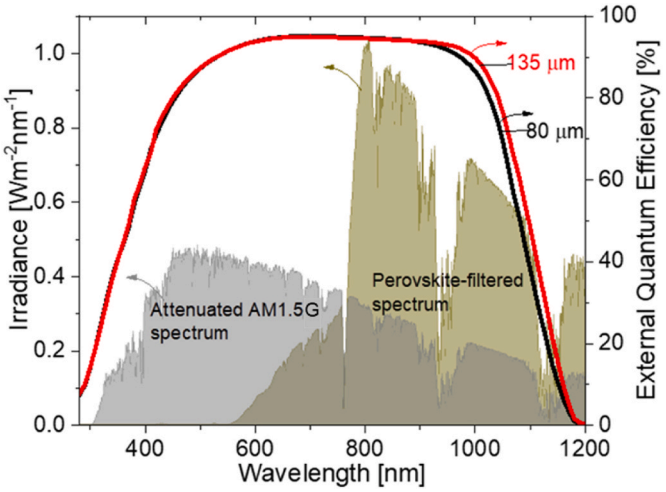

Fig. 7. Attenuated AM1.5G and perovskite-filtered irradiance spectra at the same intensity and EQE plots showing differences in infrared light absorption for 80 µm and 135 µm cells.

absorption in thin SHJ bottom cells. However, the function of antireflection coating is specific to its position in the solar cell stack. Therefore, it is likely that the coating will require re-optimization for the perovskite top cell and, at a later stage, for function in contact with encapsulation materials.

Perovskite-filtered spectra were used in our work to conduct detailed study on the potential of thin SHJ bottom cells. One fixed spectrum was used. Further optimization studies can be carried out by modifying the perovskite filtered spectrum, to emulate, for example, variations in the thickness of the perovskite top cell, or to reproduce any other variations in the top cell stack. We believe that this decoupled testing of the top and bottom cells is useful to streamline the development of Pero-Si tandems.

4. Conclusions

Large-scale production of Pero-Si tandems in the future is expected to use Si wafers thinner than 100 µm for both economic and sustainability reasons. Based on this projection, we investigate the viability of using SHJ cells fabricated on 80 µm thick wafers as bottom cells in Pero-Si tandems compared with reference cells prepared on standard 135 µm thick wafers. The use of thinner wafers for the bottom cells is associated with a decrease in infrared response while simultaneously providing greater flexibility to enhance the performance of the functional stack.

Our study addressed two crucial issues regarding thin SHJ solar cells: surface *passivation*, and *light management*. We conducted research on the consequences of thicker passivating layers in SHJ solar cells to assess the potential for passivation improvement. We analyzed the effect of technologically relevant one-dimensional ITO/MgF_2/Ag back reflector and MgF_2 antireflective coating on light management. For consistency, all cells were characterized using standard test conditions with AM1.5G irradiance, attenuated AM1.5G irradiance, and with Perovskite-filtered spectrum. The latter is the spectrum that a bottom cell would encounter in a Pero-Si tandem configuration.

As can be expected under AM1.5G standard measurements, a thicker passivating layer does not confer any particular advantage and thinner wafers show a slight decline in efficiency. While thicker passivation layers lead to an increase in series resistance and parasitic absorption, they also improve passivation, resulting in a peak V_{OC} of 747 mV in 80 µm cells and 741 mV in 135 µm cells. The best 80 µm cell of this study

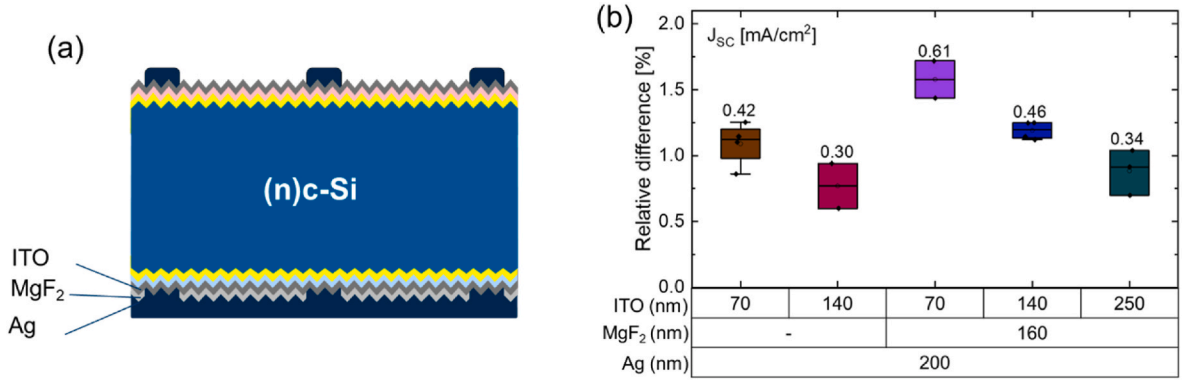

Fig. 8. (a) Schematic of SHJ solar cell showing the studied layers for back reflector; (b) Plot of relative difference in J_{SC} for various cells with different back reflector thickness combinations. Numbers in the plot indicate the absolute J_{SC} gain in mA/cm^2.

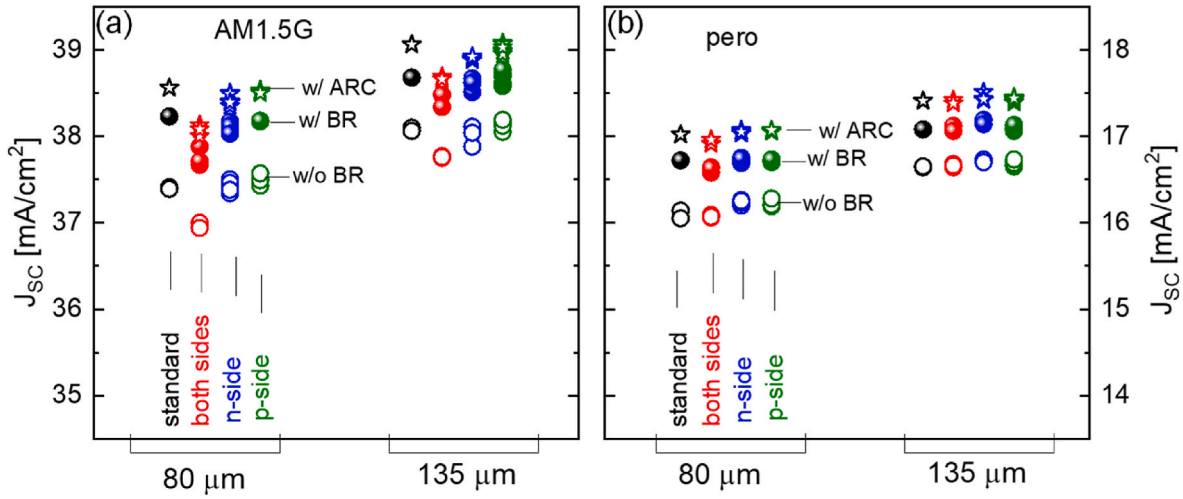

Fig. 9. Short circuit current density with and without ITO/MgF_2/Ag back reflector and after MgF_2 ARC for the various cell variations under (a) AM1.5G and (b) perovskite-filtered spectra.

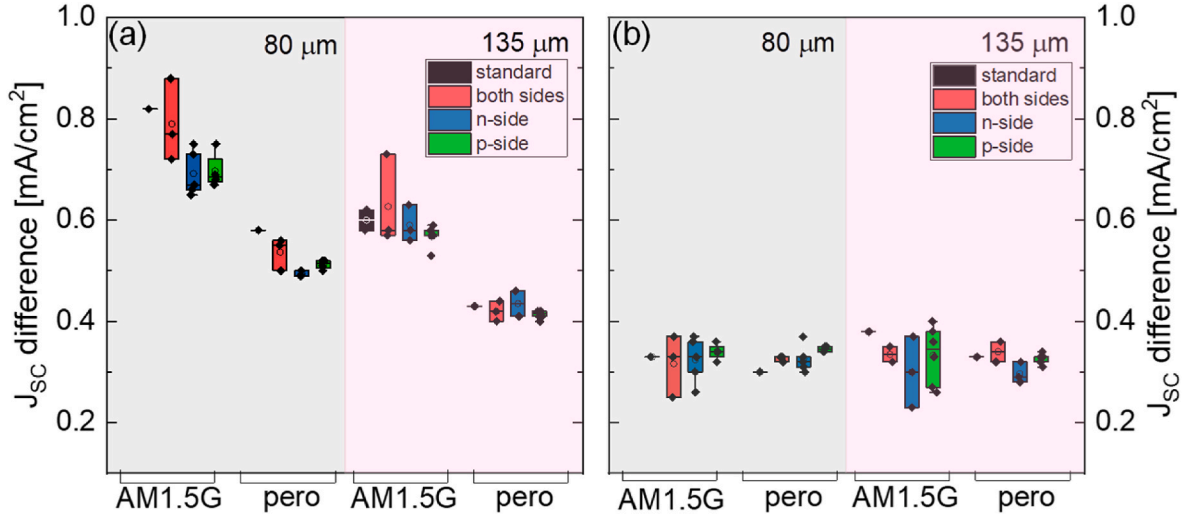

Fig. 10. Short circuit current density difference (a) with and without ITO/MgF_2/Ag back reflector and (b) before and after MgF_2 ARC for the various cell variations under AM1.5G and perovskite-filtered spectra.

had an efficiency of 23.3 % while the best 135 μm cell had an efficiency of 23.8 %.

Under lower light intensity equivalent to the conditions at the bottom cell, a significant enhancement in fill factor is observed with the thicker passivation layer. This is due to better passivation and reduced impact of the series resistance. To investigate the potential spectral

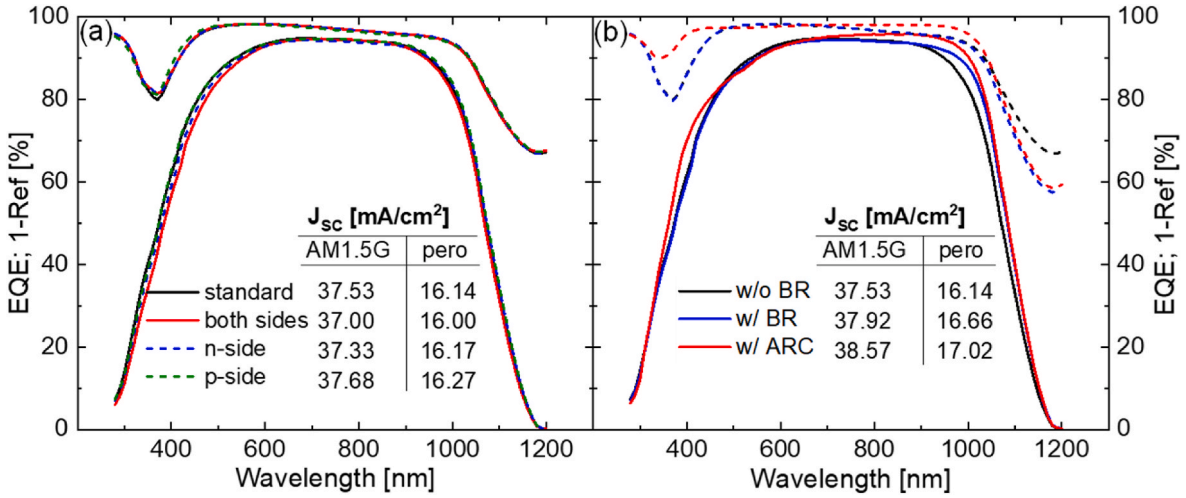

Fig. 11. External quantum efficiency and 1-Reflectance of SHJ solar cells for (a) 80 μm cells with the different passivation thickness variations and (b) 80 μm standard passivation cell without back reflector, with MgF_2/Ag back reflector and after MgF_2 anti-reflection coating.

effects on V_{OC} and *FF*, the study compared cells measured under a perovskite-filtered spectrum to those measured under the AM1.5G spectrum that was attenuated to the same photon flux (0.44 suns). Both spectra result in the same V_{OC}, p*FF*, and *FF*. This can facilitate the main optimization loop for V_{OC} and *FF* in bottom cells by simply attenuating the standard solar simulator irradiance without modifying the spectrum.

Under the Perovskite-filtered spectrum, the results indicate a favorable outcome for the SHJ cells with thinner wafers. Despite reducing the wafer thickness by 40%, there is only a minimal decrease of approximately 0.35%$_{abs}$ in the bottom cell efficiency, even without the implementation of antireflection or back reflector measures. These findings suggest that adopting 80 μm wafers is a viable approach for developing mass-produced Pero-Si tandems.

The implementation of an ITO/MgF_2/Ag back reflector and a MgF_2 anti-reflection coating can notably reduce the variation between 80 μm and 135 μm cells. Our observations indicate that the use of a back reflector leads to an increase of up to 0.58 mA/cm^2 for 80 μm solar cells under the Perovskite-filtered spectrum. In addition, 135 μm cells exhibit a gain of 0.52 mA/cm^2. Moreover, the application of the antireflective coating results in an average increase of approximately 0.3 mA/cm^2 across all cells. In total, the study exhibits a rise of 0.9 mA/cm^2 in short-circuit current density at 80 μm under the perovskite-filtered spectrum due to enhanced light management.

Our study shows that the significant decrease in wafer thickness in SHJ bottom cells for the Pero-Si tandems leads to a minor decline in power conversion efficiency. Therefore, we suggest exploring the potential benefits of Pero-Si tandems in the perovskite shadow from the SHJ bottom cell perspective. Further optimization studies can be carried out by modifying the perovskite filtered spectrum, to emulate, for example, variations in the thickness of the perovskite top cell, or to reproduce any other variations in the top cell stack.

CRediT authorship contribution statement

U. Chime: Writing – original draft, Investigation, Formal analysis, Data curation. **W. Duan:** Supervision, Methodology, Conceptualization. **A. Lambertz:** Supervision, Methodology, Conceptualization. **K. Bittkau:** Writing – review & editing, Supervision, Methodology. **V. Lauterbach:** Methodology, Data curation. **K. Ding:** Writing – review & editing, Supervision. **U. Rau:** Writing – review & editing, Supervision. **T. Merdzhanova:** Writing – review & editing, Supervision, Methodology, Formal analysis, Conceptualization. **O. Astakhov:** Writing – review & editing, Writing – original draft, Supervision, Methodology, Formal analysis, Conceptualization.

Declaration of competing interest

The authors declare that they have no known competing financial interests or personal relationships that could have appeared to influence the work reported in this paper.

Data availability

Data will be made available on request.

Acknowledgements

The authors gratefully acknowledge the European Commission under the DECADE Project (Grant agreement no: 862030). U.C is thankful to the German Academic Exchange Service (DAAD), Germany for funding. Special thanks to Alain Doumit, Sylke Lynen, Alexander Eberst, Hilde Siekmann and Wilfried Reetz for support in sample preparation and technical assistance.

References

[1] K. Yoshikawa, H. Kawasaki, W. Yoshida, T. Irie, K. Konishi, K. Nakano, T. Uto, D. Adachi, M. Kanematsu, H. Uzu, Silicon heterojunction solar cell with interdigitated back contacts for a photoconversion efficiency over 26%, Nat. Energy 2 (2017) 1–8.
[2] A. Richter, M. Hermle, S.W. Glunz, Reassessment of the limiting efficiency for crystalline silicon solar cells, IEEE J. Photovoltaics 3 (2013) 1184–1191.
[3] J.P. Mailoa, M. Lee, I.M. Peters, T. Buonassisi, A. Panchula, D.N. Weiss, Energy-yield prediction for II–VI-based thin-film tandem solar cells, Energy Environ. Sci. 9 (2016) 2644–2653.
[4] M. Jošt, E. Köhnen, A. Al-Ashouri, T. Bertram, S.p. Tomšič, A. Magomedov, E. Kasparavicius, T. Kodalle, B. Lipovšek, V. Getautis, Perovskite/CIGS tandem solar cells: from certified 24.2% toward 30% and beyond, ACS Energy Lett. 7 (2022) 1298–1307.
[5] M. Yamaguchi, F. Dimroth, J.F. Geisz, N.J. Ekins-Daukes, Multi-junction solar cells paving the way for super high-efficiency, J. Appl. Phys. 129 (2021) 240901.
[6] A.W. Ho-Baillie, J. Zheng, M.A. Mahmud, F.-J. Ma, D.R. McKenzie, M.A. Green, Recent progress and future prospects of perovskite tandem solar cells, Appl. Phys. Rev. 8 (2021) 041307.
[7] J. Li, E. Alvianto, Y. Hou, Developing the next-generation perovskite/Si tandems: toward efficient, stable, and commercially viable photovoltaics, ACS Appl. Mater. Interfaces 14 (2022) 34262–34268.
[8] F. Fu, J. Li, T.C.J. Yang, H. Liang, A. Faes, Q. Jeangros, C. Ballif, Y. Hou, Monolithic perovskite-silicon tandem solar cells: from the lab to fab? Adv. Mater. 34 (2022) 2106540.
[9] B. Chen, J.Y. Zhengshan, S. Manzoor, S. Wang, W. Weigand, Z. Yu, G. Yang, Z. Ni, X. Dai, Z.C. Holman, Blade-coated perovskites on textured silicon for 26%-efficient monolithic perovskite/silicon tandem solar cells, Joule 4 (2020) 850–864.
[10] M. De Bastiani, A.S. Subbiah, M. Babics, E. Ugur, L. Xu, J. Liu, T.G. Allen, E. Aydin, S. De Wolf, Bifacial perovskite/silicon tandem solar cells, Joule 6 (2022) 1431–1445.

[11] L.A. Zafoschnig, S. Nold, J.C. Goldschmidt, The race for lowest costs of electricity production: techno-economic analysis of silicon, perovskite and tandem solar cells, IEEE J. Photovoltaics 10 (2020) 1632–1641.
[12] A. Razzaq, T.G. Allen, W. Liu, Z. Liu, S. De Wolf, Silicon heterojunction solar cells: techno-economic assessment and opportunities, Joule 6 (2022) 514–542.
[13] Fraunhofer institute for solar energy systems photovoltaics report. https://www.ise.fraunhofer.de/content/dam/ise/de/documents/publications/studies/Photovoltaics-Report.pdf, 2023.
[14] European commission European critical raw materials act. https://single-market-economy.ec.europa.eu/publications/european-critical-raw-materials-act_en, 2023. (Accessed 21 March 2023).
[15] U. Chime, L. Wolf, V. Buga, D. Weigand, A. Gad, J. Köhler, A. Lambertz, W. Duan, K. Ding, T. Merdzhanova, How thin practical silicon heterojunction solar cells could Be? Experimental study under 1 sun and under indoor illumination, Sol. RRL 6 (2022) 2100594.
[16] H. Sai, H. Umishio, T. Matsui, S. Nunomura, T. Kawatsu, H. Takato, K. Matsubara, Impact of silicon wafer thickness on photovoltaic performance of crystalline silicon heterojunction solar cells, Jpn. J. Appl. Phys. 57 (2018) 08RB10.
[17] H. Sai, T. Oku, Y. Sato, M. Tanabe, T. Matsui, K. Matsubara, Potential of very thin and high-efficiency silicon heterojunction solar cells, Prog. Photovoltaics Res. Appl. 27 (2019) 1061–1070.
[18] H. Sai, Y. Sato, T. Oku, T. Matsui, Very thin crystalline silicon cells: a way to improve the photovoltaic performance at elevated temperatures, Prog. Photovoltaics Res. Appl. (2021) 1–12.
[19] A. Augusto, P. Balaji, J. Karas, S.G. Bowden, Impact of substrate thickness on the surface passivation in high performance n-type solar cells, in: 2018 IEEE 7th World Conference on Photovoltaic Energy Conversion (WCPEC) (A Joint Conference of 45th IEEE PVSC, 28th PVSEC & 34th EU PVSEC), 2018, pp. 2792–2794.
[20] D. Zhang, M. Najafi, V. Zardetto, M. Dörenkämper, X. Zhou, S. Veenstra, L. Geerligs, T. Aernouts, R. Andriessen, High efficiency 4-terminal perovskite/c-Si tandem cells, Sol. Energy Mater. Sol. Cell. 188 (2018) 1–5.
[21] M.A. Green, Limiting efficiency of bulk and thin-film silicon solar cells in the presence of surface recombination, Prog. Photovoltaics Res. Appl. 7 (1999) 327–330.
[22] J. Panigrahi, V.K. Komarala, Progress on the intrinsic a-Si: H films for interface passivation of silicon heterojunction solar cells: a review, J. Non-Cryst. Solids 574 (2021) 121166.
[23] X. Zhang, A. Cuevas, B. Demaurex, S. De Wolf, Sputtered hydrogenated amorphous silicon for silicon heterojunction solar cell fabrication, Energy Proc. 55 (2014) 865–872.
[24] A. Kanevce, W.K. Metzger, The role of amorphous silicon and tunneling in heterojunction with intrinsic thin layer (HIT) solar cells, J. Appl. Phys. 105 (2009) 094507.
[25] P. Balaji, W.J. Dauksher, S.G. Bowden, A. Augusto, Improving surface passivation on very thin substrates for high efficiency silicon heterojunction solar cells, Sol. Energy Mater. Sol. Cell. 216 (2020) 110715.
[26] M. Leilaeioun, W. Weigand, M. Boccard, J.Y. Zhengshan, K. Fisher, Z.C. Holman, Contact resistivity of the p-type amorphous silicon hole contact in silicon heterojunction solar cells, IEEE J. Photovoltaics 10 (2019) 54–62.
[27] N.v. Reich, W. Van Sark, E. Alsema, R. Lof, R. Schropp, W. Sinke, W. Turkenburg, Crystalline silicon cell performance at low light intensities, Sol. Energy Mater. Sol. Cell. 93 (2009) 1471–1481.
[28] K. Rühle, M.K. Juhl, M.D. Abbott, M. Kasemann, Evaluating crystalline silicon solar cells at low light intensities using intensity-dependent analysis of I–V parameters, IEEE J. Photovoltaics 5 (2015) 926–931.
[29] R. Saive, Light trapping in thin silicon solar cells: a review on fundamentals and technologies, Prog. Photovoltaics Res. Appl. 29 (2021) 1125–1137.
[30] P. Pathi, A. Peer, R. Biswas, Nano-photonic structures for light trapping in ultra-thin crystalline silicon solar cells, Nanomaterials 7 (2017) 17.
[31] H.-S. Kim, D.B. Patel, H. Kim, M. Patel, K.R. Chauhan, W. Park, J. Kim, Electrical and optical properties of Si microwire solar cells, Sol. Energy Mater. Sol. Cell. 164 (2017) 7–12.
[32] P. Bermel, C. Luo, L. Zeng, L.C. Kimerling, J.D. Joannopoulos, Improving thin-film crystalline silicon solar cell efficiencies with photonic crystals, Opt Express 15 (2007) 16986–17000.
[33] L. Zeng, P. Bermel, Y. Yi, B. Alamariu, K. Broderick, J. Liu, C. Hong, X. Duan, J. Joannopoulos, L. Kimerling, Demonstration of enhanced absorption in thin film Si solar cells with textured photonic crystal back reflector, Appl. Phys. Lett. 93 (2008) 221105.
[34] W. Duan, A. Lambertz, K. Bittkau, D. Qiu, K. Qiu, U. Rau, K. Ding, A route towards high-efficiency silicon heterojunction solar cells, Prog. Photovoltaics Res. Appl. 30 (2022) 384–392.
[35] F.-J. Haug, T. Söderström, O. Cubero, V. Terrazzoni-Daudrix, C. Ballif, Plasmonic absorption in textured silver back reflectors of thin film solar cells, J. Appl. Phys. 104 (2008).
[36] A. Eberst, A. Zamchiy, K. Qiu, P. Winkel, H.T. Gebrewold, A. Lambertz, W. Duan, S. Li, K. Bittkau, T. Kirchartz, Optical optimization potential of transparent-passivated contacts in silicon solar cells, Sol. RRL 6 (2022) 2101050.
[37] F. Sahli, J. Werner, B.A. Kamino, M. Bräuninger, R. Monnard, B. Paviet-Salomon, L. Barraud, L. Ding, J.J. Diaz Leon, D. Sacchetto, Fully textured monolithic perovskite/silicon tandem solar cells with 25.2% power conversion efficiency, Nat. Mater. 17 (2018) 820–826.
[38] D.L. Staebler, C. Wronski, Reversible conductivity changes in discharge-produced amorphous Si, Appl. Phys. Lett. 31 (1977) 292–294.
[39] P. Mahtani, R. Varache, B. Jovet, C. Longeaud, J.-P. Kleider, N.P. Kherani, Light induced changes in the amorphous—crystalline silicon heterointerface, J. Appl. Phys. 114 (2013) 124503.